

9. Hays, J., Imbrie, J. & Shackleton, N. J. *Science* **194**, 1121-1132 (1976).
 10. Lambracherie, M. *Paleoceanography* **4**, 629-638 (1989).

ACKNOWLEDGEMENTS. We thank W. Broecker, G. Kukla and D. Peteet for their comments, G. Mathieu for radiocarbon analyses, and W. Woelfli and G. Bonani for obtaining the AMS date. We acknowledge the support of the Lamont-Doherty Geological Observatory of Columbia University, and the NSF (S.S.). Lamont-Doherty Contribution No. 4609.

Eustatic sea level fluctuations induced by polar wander

Roberto Sabadini*, Carlo Doglioni† & David A. Yuen‡

* Dipartimento di Fisica, Settore Geofisica, Università di Bologna, Viale B Pichat, 8, 40127 Bologna, Italy

† Dipartimento di Scienze Geologiche e Paleontologiche, Università di Ferrara, Corso Ercole I D'Este, 32, 44100 Ferrara, Italy

‡ Minnesota Supercomputer Institute and Department of Geology and Geophysics, University of Minnesota, Minneapolis, Minnesota 55415, USA

THE observation of apparently simultaneous episodes of deposition or non-deposition of marine sediments in different parts of the world has led to the proposal that at least some sea level rises and falls must be global, or eustatic, in character¹⁻³. Here we show that polar wander of a viscoelastic stratified Earth can induce global sea level fluctuations comparable to the short-term component in the eustatic sea-level curves. The sign of these fluctuations, which are very sensitive to the rheological stratification, depends on the geographical location of the observation point; rises and falls in sea level can thus be coeval in different parts of the world. This finding is in distinct contrast to the main assumption underlying the reconstruction of eustatic curves, namely that global sea-level events produce the same depositional sequence everywhere. This apparent contradiction is due to the poor time resolution of the stratigraphic records in the distant past, which is comparable to the timescale of polar motion⁴⁻⁶, and to non-uniform data coverage. We propose that polar wander should be added to the list of geophysical mechanisms (the others are glacial instabilities, plate tectonic mechanisms, sea-floor spreading, and thermal and compaction-induced subsidence) that can control the third-order cycles in sea level.

Sea level fluctuations, due to variations in the centrifugal force associated with long-term wander of the Earth's rotation axis, can be predicted theoretically from a radially stratified viscoelastic Earth model⁷. The possible causes for these long-term displacements of the axis of rotation can originate in the mantle, as suggested by the rotational responses of the Earth to the anomalous density heterogeneities inferred from seismic tomography^{8,9}, or can be caused by the surface redistribution of melt water from ice ages¹⁰. Here we shall disregard the possible dynamical sources of polar wander and focus instead on the effects induced by rates of polar motion, the amplitude of which is selected to be in agreement with recent analyses of palaeomagnetic data¹¹. In the Laplace transform domain, the perturbation in the centrifugal potential depends, to first order, on the direction cosines of the rotation axis $m(s) = m_1(s) + im_2(s)$

$$\psi(s) = -\sqrt{2\pi/15}\Omega^2 a^2 m(s) Y_2^1(\theta, \phi) \quad (1)$$

where Ω is the rotation rate of the Earth, a is the Earth's radius, Y_2^1 is the spherical harmonic and θ, ϕ are the colatitude and longitude, respectively.

Because our model is radially symmetric, and the distribution of the ocean is assumed uniform, this $l=2, m=1$ perturbative potential induces a signal in the relative sea level fluctuation ξ of the same angular degree and order. Lateral variations in viscosity would contaminate this signal with shorter wavelengths. We have then

$$\xi_2^1(s) = (1 + k_2^T(s) - h_2^T(s))\psi(s)/g \quad (2)$$

where k_2^T, h_2^T are the $l=2$ components of the tidal Love numbers for the gravitational potential and vertical displacement respectively and g is the gravitational acceleration. This expression of the sea level change relative to the sea bottom does not account for the effects of self-attraction of the uniform ocean¹². This effect can be easily seen to produce an increase of at most 10 per cent on our results. The term $(1 + k_2^T(s))$ yields the deformation of the ocean surface relative to the Earth's centre, whereas $h_2^T(s)$ controls the vertical displacement of the sea bottom. Owing to the lag between these two contributions, perturbations in the centrifugal potential induce sea level fluctuations, as shown by the drawing in Fig. 1. The white arrow indicates the direction of the polar wander, and the solid and dashed curves depict the shift of the equipotential surface (geoid). Highstands and lowstands are generated, depending on the latitude and longitude of the observation points with respect to the polar motion. To quantify these sea level fluctuations, we consider the spectral decomposition of the tidal Love numbers

$$k_2^T(s) = k_e^T + \sum_{i=1}^M k_i^T/(s - s_i) \quad (3)$$

$$h_2^T(s) = h_e^T + \sum_{i=1}^M h_i^T/(s - s_i) \quad (4)$$

where k_e^T and h_e^T represent the elastic contributions, M denotes the number of relaxation modes associated with the Earth model, s_i and k_i^T, h_i^T their inverse relaxation times and strengths⁷. Our model consists of a uniform elastic lithosphere of 100 km, two viscoelastic Maxwell layers, with viscosities ν_1 and ν_2 , modelling the upper and lower mantle and an inviscid core⁷. The interface separating the upper and lower mantle is located at a depth of 670 km, and appropriate boundary conditions for the normal stress at this interface are used to reproduce the mechanical behaviour of phase-change or chemical transitions, which are assumed fully adiabatic and non-adiabatic respectively^{8,9}. In what follows, we study the responses of the Earth subject to a constant polar wander of 1° Myr^{-1} ; this value is a lower bound, a deduced from palaeomagnetic observations^{6,11} and these results can be extended to higher polar drift rates by linear scaling.

In Fig. 2 the perturbative potential is applied at time $t=0$; we follow the evolution of the sea level at mid-latitudes, where the effects are larger owing to the Y_2^1 dependence of the perturba-

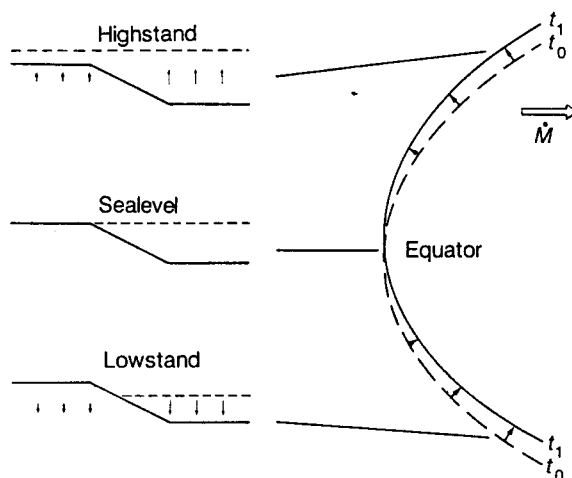


FIG. 1 Pictorial representation of sea level fluctuation induced by polar wander. The white arrow denotes the direction of polar drift, at a rate $\dot{M} = 1^\circ \text{ Myr}^{-1}$. The solid and dashed curves represent the deformation of geoid and topography of the sea floor at times $t = t_0$, when the perturbation is initially imposed and a subsequent time $t = t_1$. Sea level is unperturbed at the Equator but rises and falls occur in the Northern and Southern Hemispheres, respectively.

tion. It is quite remarkable that sea level fluctuations are extremely sensitive to viscosity stratification and lithospheric thickness. These curves are characterized by transient behaviour, more pronounced for high lower-mantle viscosities, followed by a linear trend, which is connected with a constant rate of polar wander¹⁰. For smooth viscosity contrasts, phase-change models (dashed curves), produce a smaller signal than chemically stratified ones (solid curves). For the chemically stratified models, deflections of the 670-km discontinuity induce a buoyant restoring force which inhibits viscous relaxation in the mantle. This, in turn, reduces the vertical uplift of the sea floor and helps to maintain the offset between the sea-floor topography and the geoid. Recent work by Gurnis¹³ has emphasized the importance in the trade-off between the dynamically induced topography and the geoid in the flooding of continental platforms. For high viscosity contrasts ($\nu_2 = 10^{23}$ Pa s), the stiffening of the lower mantle overcomes the dynamical effects associated with the nature of the 670-km discontinuity. Thus phase-change and chemically stratified models exhibit the same behaviour. The dotted curve, corresponding to a model with a reduced lithospheric thickness of 50 km, shows the sensitivity of sea level fluctuations induced by polar wander to variations in lithospheric thickness. Recent analyses of geoid anomalies¹⁴ and post-glacial rebound^{15,16} favour high viscosity contrasts. These models then predict sea level fluctuations of the order of several tens of metres on timescales of 10^6 yr, which are comparable to the third-order cycle in the eustatic curves.

It is useful to analyse the behaviour of the rate of sea level fluctuations (Fig. 3). Rates of the order of 0.05–0.1 mm yr⁻¹ are maintained for timescales of 0.5 Myr if the viscosity contrast is sufficiently high ($\nu_2/\nu_1 = 50$ to 100). For uniform models, or mild viscosity contrasts ($\nu_2/\nu_1 = 1$ to 10), rates of sea level fluctuations decay in a few tens of thousand years. After the decay of the initial transient, the rates reach a final value of ~ 0.02 mm yr⁻¹, irrespective of the rheological stratification. As expected, phase-change models produce lower rates, except for

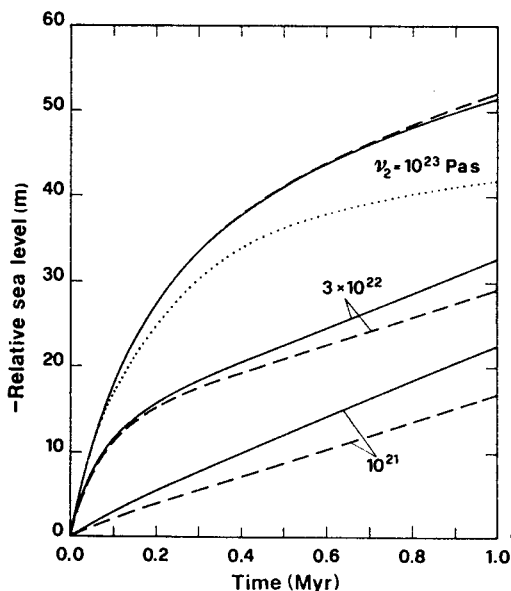


FIG. 2 Time dependence of relative sea level fluctuations at mid-latitudes ($\theta = 45^\circ$ N, $\phi = 0^\circ$), corresponding to $\dot{M} = 1^\circ \text{ Myr}^{-1}$ and polar motion toward Greenwich. The perturbative potential is applied at time $t = 0$. Solid curves correspond to chemically stratified models (fully non-adiabatic) and dashed ones correspond to fully adiabatic phase changes. Lithosphere thickness is 100 km, except for the dotted curve, which corresponds to 50 km. The upper-mantle viscosity ν_1 is 10^{21} Pa s, and the lower mantle is varied from 10^{21} Pa s (bottom) to 10^{23} Pa s (top).

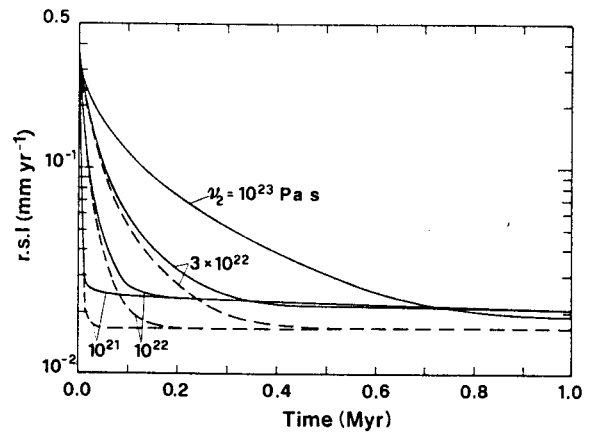


FIG. 3 Time dependence of relative sea level (r.s.l.) in mm yr⁻¹. Solid curves correspond to chemically stratified models and dashed ones correspond to fully adiabatic phase changes. For $\nu_2 = 10^{23}$ Pa s, the chemical transition and phase-change models are indistinguishable. Results for $\nu_2 = 10^{22}$ Pa s are also shown.

high viscosity contrasts, in which case these models are indistinguishable from chemically stratified ones. We find that rates of sea level fluctuations are around one order of magnitude smaller than those associated with vertical deformation of the sea floor which are ~ 1 –1.5 mm yr⁻¹. This value agrees with the estimates, made by Hanada¹⁷ from the readjustment of the Earth rotational bulge, driven by polar wander. Rates of the order of 0.1–0.5 mm yr⁻¹ in the initial state of polar wander, are also consistent with that obtained by Han and Wahr¹⁸ who were the first to account for the effects induced by a variable centrifugal potential on post-glacial rebound within the framework of a viscoelastic mantle.

The rates predicted by our model are of the same order of magnitude as the short-wavelength ones associated with temporal variations of the horizontal tectonic stress field in the lithosphere¹⁹. From these results, it is clear that the proposed mechanism of polar wander is efficient in inducing sea level fluctuations especially during epochs of rotational instabilities, caused by mantle flows. Significant shift of the rotation pole occurred, for example, during the Late Cretaceous^{6,11,20}. Other effects from lateral variations in the mantle viscosity structure would act to produce eustatic sea level changes with higher-degree harmonics than $l = 2$. Therefore our findings indicate that the highstand or lowstand system tracts observed in one part of the world are not necessarily correlated with the same depositional sequence in another geographical location. A highstand in a marine package in the Northern Hemisphere can, in fact, be coeval with a lowstand in the Southern Hemisphere at the same longitude if the only active mechanism that induced the eustatic sea-level event was polar wander. There is thus an urgent need to improve the temporal resolution of sequence stratigraphy by about one order of magnitude so that eustatic sea-level events in sedimentary packages from different parts of the world are recognized accurately. □

Received 2 February; accepted 20 April 1990.

1. Haq, B. U., Hardenbol, J. & Vail, P. R. *Science* **235**, 1156–1167 (1987).
2. Fischer, A. G. *Climate in Earth History, Studies in Geophysics* 97–104 (Natl. Acad. Press, Washington, DC, 1982).
3. Goldammer, R. K., Dunn, P. A. & Hardie, L. A. *Am. J. Sci.* **287**, 853–892 (1987).
4. Miller, K. G. & Kent, D. V. *Cushman Foundation for Foraminiferal Research, Spec. Publ.* **24**, 51–56 (1987).
5. Vail, P. R. et al. *Am. Ass. Petrol. Geol. Mem.* **26**, 49–212 (1977).
6. Gordon, R. G. *Rev. Earth planet. Sci.* **15**, 567–593 (1987).
7. Yuen, D. A., Sabadini, R. & Boschi, E. *J. geophys. Res.* **87**, 10745–10762 (1982).
8. Sabadini, R. & Yuen, D. A. *Nature* **339**, 373–375 (1989).

9. Ricard, Y. & Sabadini, R. *Geophys. Res. Lett.* **17**, 627-630 (1990).
10. Sabadini, R., Yuen, D. A. & Boschi, E. *Nature* **296**, 338-341 (1982).
11. Gordon, R. G. & Livermore, R. A. *Geophys. J. R. astr. Soc.* **91**, 1049-1057 (1987).
12. Dahlen, F. A. *Geophys. J. R. astr. Soc.* **46**, 363-406 (1976).
13. Gurnis, M. K. *Nature* **344**, 754-756 (1990).
14. Ricard, Y., Vigny, C. & Froidevaux, C. *J. geophys. Res.* **94**, 13739-13754 (1989).
15. Yuen, D. A., Sabadini, R., Gasperini, P. & Boschi, E. *J. geophys. Res.* **91**, 11420-11438 (1986).
16. Nakada, M. & Lambeck, K. *Geophys. J.* **96**, 497-517 (1989).
17. Hanada, H. *Geophys. J.* **95**, 315-321 (1988).
18. Han, D. & Wahr, J. *Geophys. Monogr. Ser.* **49**, Vol. 4, 1-6.
19. Cloetingh, S., Lambeck, K. & McQueen, H. *Petroleum Geology of North West Europe* (eds Brooks, J. & Glennie, K.) 49-57 (Graham & Trotman, 1987).
20. Sager, W. W. & Bleil, U. *Nature* **326**, 488-490 (1987).

ACKNOWLEDGEMENTS. We thank R. Gordon for stimulating conversations which helped us in this work. This work was supported by the Agenzia Spaziale Italiana and NASA.

Model of carbon fixation in microbial mats from 3,500 Myr ago to the present

Lynn J. Rothschild & Rocco L. Mancinelli

Solar System Exploration Branch, Mail Stop 239-12,
NASA-Ames Research Center, Moffet Field, California 94035, USA

BIOLOGICAL carbon fixation is an important part of global carbon cycling and ecology. Fixation that took place 3,500 million years ago is recorded in the laminated sedimentary rock structures known as stromatolites, which are fossilized remains of microbial mat communities¹⁻⁴. Stromatolites are the most abundant type of fossil found in the Proterozoic (2,500 to 590 Myr ago), but they then declined, possibly because of predation and competition^{5,6}. Using modern microbial mats as analogues for ancient stromatolites, we show that the rate of carbon fixation is higher at the greater levels of atmospheric CO₂ that were probably present in the past⁷. We suggest that carbon fixation in microbial mats was not carbon-limited during the early Precambrian, but became carbon-limited as the supply of inorganic carbon decreased⁸. Carbon limitation led to a lower rate of carbon fixation, especially towards the end of the Precambrian. Thus, another reason for the decline of the stromatolites could have been a decrease in available CO₂.

The microbial mat systems studied are located in evaporation ponds of the salt company Exportadora de Sal, SA (Fig. 1). One study site was located in evaporation pond 5 (2,295 hectare, ~1 m in depth, 5-10% NaCl) ~2 km east of the outflow gate from pond 5 to 6. The bottom of pond 5 is covered by a laminated microbial mat consisting of, from top to bottom, diatoms (0-2 mm) (L.J.R., unpublished observations), cyanobacteria dominated by *Microcoleus chthonoplastes* (1-2 mm), and layers composed of prokaryotes living heterotrophically under anaerobic conditions (~3 cm) (refs 9-11). The other mat communities live in the intertidal area of Laguna Ojo de Liebre (Fig. 1). Both were cyanobacterial, one dominated by *Lyngbya aestuarii*, the other by *Calothrix crustacea* (~2-5 mm in thickness).

Initial experiments were conducted on 2-4 June 1989 in all three mat communities, and repeated for the *Lyngbya* mats on 2 November 1989. Carbon fixation rates were obtained under different levels of dissolved inorganic carbon (DIC) ranging from ~2 mM (ambient) to 252 mM. Environmental parameters during the experiments are described in Table 1. We conducted all experiments during the middle of the day when light levels were essentially constant and, to insure that our observations were not the result of a light-level effect, experiments were run at random. Mat samples were incubated *in situ* in bottomless clear glass serum vials (125 ml; cross-sectional area, 17.2 cm²) sealed with a syringe septum. The vials were inserted into the mat in such a way that the bottle was filled with air. Pond or lagoon water (DIC ≈ 2 mM, ~pH 7.2), or water with supplement-

tary NaHCO₃ (~pH 7.2), was spiked with NaH¹⁴CO₃ (ICN Biomedicals or New England Nuclear) to a final concentration of 1-2 μCi ml⁻¹ and injected into the bottles. Samples were removed periodically at times of up to 60 min and immediately frozen on dry ice. On return to the laboratory, the samples were defrosted, homogenized in a buffer (100 mM Tris buffer, pH 8; 50 mM EDTA) and sonicated on ice. Two aliquots were placed in separate scintillation vials where they were acidified, dried, dissolved in warm water and counted in Ecolume (ICN Biomedicals). All counts were adjusted with internal standards. All experiments were performed in triplicate.

Carbon fixation rates were essentially linear over 60 min, but we did observe variations attributable to such factors as fluctuations in light level due to small clouds passing overhead. Also, experiments on pond 5 mat have shown that within 20 min of fixation, some portion of the newly fixed carbon is remineralized by respiration (data not shown). After this time, the counteracting forces of carbon fixation and respiration make it difficult to determine carbon fixation rates alone. To minimize the impact of respiration on the pool of acid-stable carbon, the shortest incubation time experimentally feasible, 15 min, was used to calculate carbon uptake rates.

Carbon fixation rates were calculated from total acid-stable counts in the duplicate aliquots from each of the triplicate experimental samples, excluding both the highest and lowest count. Carbon fixation rates of pond 5 and *Lyngbya* mats, expressed as μg carbon fixed m⁻² min⁻¹ and graphed as a function of DIC, are shown in Fig. 2a. Results for *Calothrix* mats were similar (data not shown). Standard deviations for each rate measurement averaged 11% for *Lyngbya* samples and 15% for pond 5. Carbon fixation rates for pond 5 and *Lyngbya* mats attain a maximum at ~50 mM DIC. These data are consistent with studies¹² on a pure culture of the cyanobacterium *Synechococcus* which showed that photosynthesis probably becomes saturated with respect to inorganic carbon at DIC levels just over 25 mM.

Current astrophysical models suggest that the Sun has increased in luminosity since the origin of the Solar System. To account for the presence of liquid water on the early Earth in spite of a lower solar luminosity, Owen *et al.*⁷ proposed that a higher level of CO₂ in the past created a greenhouse effect, thus raising the surface temperature of the Earth. If this widely accepted hypothesis is correct, it implies correspondingly higher levels of DIC in ancient oceans. Pollack *et al.*¹³ have calculated the DIC levels in a hypothetical ocean as a function of pCO₂, assuming an isothermal ocean (5°C) with a salinity of 3.5%

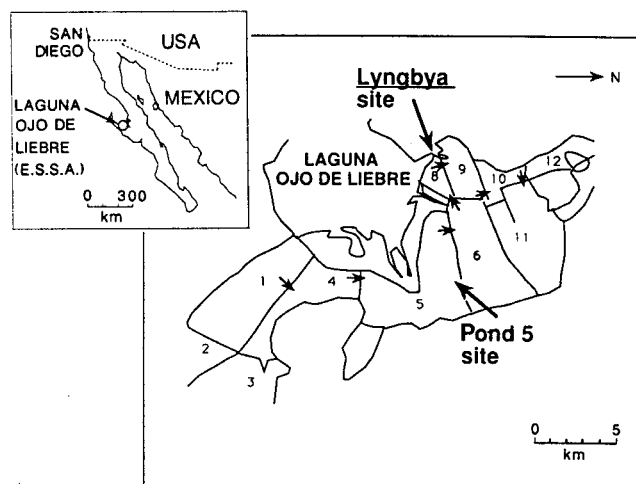


FIG. 1 Map showing location of study sites. Small arrows indicate the direction of water flow through the gates connecting evaporation ponds.